

# Phase and Shape Dependent Photoactivity of Titania for Nitroaromatics Reduction Under UV Light Irradiation

Jaspreet Kaur and Bonamali Pal\*

School of Chemistry and Biochemistry, Thapar Institute of Engineering and Technology, Patiala 147004, Punjab, India

This work describes importance of TiO<sub>2</sub> nanostructures of different shapes (nanospheres and nanorods) and crystal phases (anatase and rutile) for the photoreduction of nitroaromatics into corresponding aminoaromatics under UV light irradiation. Anatase nanoparticles were most active of all the catalysts due to the superior stability of this phase and comparatively the rutile nanorods ( $L \times W = 28\text{--}30\text{ nm} \times 3.5\text{--}3.8\text{ nm}$ ) showed superior photoactivity (~3 times) as compared to rutile nanospheres of size 122 nm for the photoreduction due to electron transport along longitudinal length, larger surface area (69 m<sup>2</sup>g<sup>-1</sup>), quenched PL emission, increased lifetime of charge carriers (1.8 ns) of rutile nanorods as compare to rutile nanospheres having lower surface area (18 m<sup>2</sup>g<sup>-1</sup>) and charge carrier lifetime (1.1 ns). The overall rate of reduction/hour for *m*-NBA and *m*-NT photoreduction with all of these catalysts has been found to vary in the following order ANP > P25-TiO<sub>2</sub> > RNR > ANR > RNP.

**Keywords:** Different Polymorphs of TiO<sub>2</sub>, Rutile and Anatase Nanorods, Photoluminescence Quenching, Enhanced Life Time of Excitons, Nitroaromatic Reduction.

## 1. INTRODUCTION

Titanium dioxide (TiO<sub>2</sub>) semiconductor nowadays is used for greener synthesis of aminoaromatics by one step reduction<sup>1-4</sup> of nitroaromatics. The production of aminoaromatics from nitroaromatics is of great interest because aminoaromatics are important intermediates for the synthesis<sup>5-8</sup> of dyes, antioxidants, herbicides, polymers, pharmaceuticals and other fine chemicals. These can be prepared easily by the reduction of nitroaromatics using catalytic hydrogenation, zinc, tin, iron, Au/SiO<sub>2</sub>, Au/Al<sub>2</sub>O<sub>3</sub>, Pd/TiO<sub>2</sub>, Pt–Ni bimetallic nanoparticles<sup>8-15</sup> and Pt–TiO<sub>2</sub> a variety of other reduction conditions. The drawbacks of all these methods include the requirement of toxic solvents, strong reducing agents like NaBH<sub>4</sub>, expensive metals like Au/Pt, reactions at high pressure and temperature and generation of toxic byproducts. Whereas the use of titania for the photoreduction of nitroaromatics is highly advantageous over all these methods because it is a cheap, non-toxic, generates no harmful byproduct and require room temperature and pressure conditions. Also, conduction band energy of TiO<sub>2</sub> is –0.85 V in comparison to –0.5 V versus SCE of the –NO<sub>2</sub> group, so NO<sub>2</sub> is preferably reduced<sup>16-20</sup> over aceto, cyano, and aldehyde functionality present in the same compound.

It is reported that anatase TiO<sub>2</sub> usually shows much higher photocatalytic activity than rutile TiO<sub>2</sub>. However, some recent reports show the improved selectivity of rutile TiO<sub>2</sub> nanoparticles<sup>21-24</sup> for selective oxidation of aromatic alcohols to aldehydes, photoreduction of nitroaromatics to aminoaromatics such as *m*-nitrotoluene photoreduction to *m*-aminotoluene. Further, it is reported<sup>25</sup> that rutile nanoparticles show 100% yield and selectivity of *m*-dinitrobenzene photoreduction to *m*-nitroaniline. Also, metal (coinage and platinum group) loading also improves the selectivity of P25-TiO<sub>2</sub> for the photoreduction of *m*-dinitrobenzene<sup>26</sup> while metal loading does not shows significant improvement in rutile TiO<sub>2</sub> nanoparticles photoactivity.

Further, the photocatalytic activity of anatase and rutile nanoparticles can also be improved by changing their morphology<sup>27-30</sup> from spherical to rod. The advantages of one-dimensional nanorods over nanospheres as photocatalyst are that the one-dimensional geometry facilitates fast and long distance electron transport, exhibit higher specific surface area, light absorption increases because of the larger length-to-diameter ratio. The improved photoactivity of rutile nanorods<sup>31</sup> has been observed for Rhodamine B degradation (low temp) and gas-phase decomposition of acetaldehyde. Herein, we investigated the potential application of anatase and rutile titania

\*Author to whom correspondence should be addressed.

nanorods and nanospheres for the improved photoreduction of nitroaromatics such as *m*-nitrobenzoic acid (*m*-NBA) and *m*-nitrotoluene (*m*-NT).

## 2. EXPERIMENTAL DETAILS

### 2.1. Materials

Degussa P25 TiO<sub>2</sub>, titanium tetrachloride, titanium(IV) isopropoxide, *m*-nitrobenzoic acid (C<sub>7</sub>NO<sub>4</sub>H<sub>5</sub>), *m*-aminobenzoic acid (C<sub>7</sub>NO<sub>2</sub>H<sub>7</sub>), *m*-nitrotoluene (C<sub>7</sub>NO<sub>2</sub>H<sub>7</sub>), *m*-toluidine (C<sub>7</sub>NH<sub>9</sub>), nitric acid, isopropanol, methanol were purchased from Loba Chemicals and used without further purification. Deionized water was obtained using an ultra filtration system (Milli-Q, Milipore) with a measured conductivity of 35 mho cm<sup>-1</sup> at 25 °C.

### 2.2. Synthesis of Anatase Nanorods (ANR)

ANR were synthesized by a hydrothermal method as reported<sup>32</sup> elsewhere. Briefly, 4.73 g of P25-TiO<sub>2</sub> was mixed with 72 ml of NaOH (10 N) and then subjected to hydrothermal treatment at 130 °C in a Teflon lined autoclave (80 ml capacity) for 20 h. The obtained slurry was washed repeatedly with 0.1 N HNO<sub>3</sub>, followed by water and methanol, and dried in a hot air oven at 70–80 °C for 3 h. 3.2 g of obtained particles were further dissolved in 64 mL of water and the resulted slurry (pH = 5.6) was autoclaved at 175 °C for 48 h. Thus obtained ANR were filtered, washed with distilled water and methanol, and dried in hot air oven at 70–80 °C for 3 h.

### 2.3. Synthesis of Anatase Nanospheres (ANP)

ANS were synthesized by sol-gel<sup>33</sup> method. Typically, 0.1 M titanium(IV) isopropoxide solution was prepared in 150 mL of iso-propanol. Another solution of measured quantity of water and 150 mL iso-propanol was also prepared. Both solutions were sealed and subjected to rapid magnetic stirring so as to obtain homogeneous mixtures. The water solution was then added drop wise to the 0.1 M titanium(IV) isopropoxide solution under continuous magnetic stirring for 5 h. This resulted into hydrolysis of titanium(IV) isopropoxide and white colored precipitates were formed. These as obtained precipitates were filtered and washed thrice with deionized water and dried in hot air oven at 80 °C. The powder thus obtained was calcined at 450 °C for 2 h and named as ANP catalyst.

### 2.4. Synthesis of Rutile Nanospheres (RNP)

RNS were synthesized by the calcination of commercially available Degussa P25 TiO<sub>2</sub> powder at 800 °C in a muffle furnace for 2 h.

### 2.5. Synthesis of Rutile Nanorods (RNR)

RNR were synthesized through a seed-mediated growth process<sup>34</sup> by hydrolysing TiCl<sub>4</sub> in highly acidic aqueous

solution. Typically, 20 mL of aqueous TiCl<sub>4</sub> (3 M) was added into 35 mL of nitric acid solution (15 M). The mixture was refluxed for 24 h at 120 °C. The residue thus obtained was centrifuged, washed three times with dilute nitric acid solution at pH = 1. The centrifuged solid was then redispersed in dilute nitric acid solution (6 mL) at pH = 1.

Then a growth solution of dilute TiCl<sub>4</sub> (0.3 M) was prepared and 20 mL of it was added into above seed solution and refluxed for 24 h at 120 °C. The residue thus obtained was centrifuged, washed as mentioned above and dried in hot air oven at 70–80 °C for 3–4 h.

### 2.6. Characterization Techniques

The optical absorption spectra of as synthesized TiO<sub>2</sub> samples were recorded with a diffuse reflectance spectrophotometer by Avantes using BaSO<sub>4</sub> as reflectance standard. Photoluminescence (PL) spectra were recorded by using a spectrofluorimeter by Perkin-Elmer LS55 at room temperature on excitation with xenon lamp ( $\lambda_{\text{ext}}$ ) at 320 nm in ethanol suspension. Transmission electron microscope (TEM) photographs were taken on the Hitachi 7500 model with resolution 2 Å operating at voltage 120 kV. The crystallographic studies have been carried out by using X-ray diffractometer by PANalytical X'Pert PRO with Cu-K $\alpha$  ( $k = 1.54060$  Å) radiation operated at 45 kV. The specific surface area was determined by N<sub>2</sub> adsorption

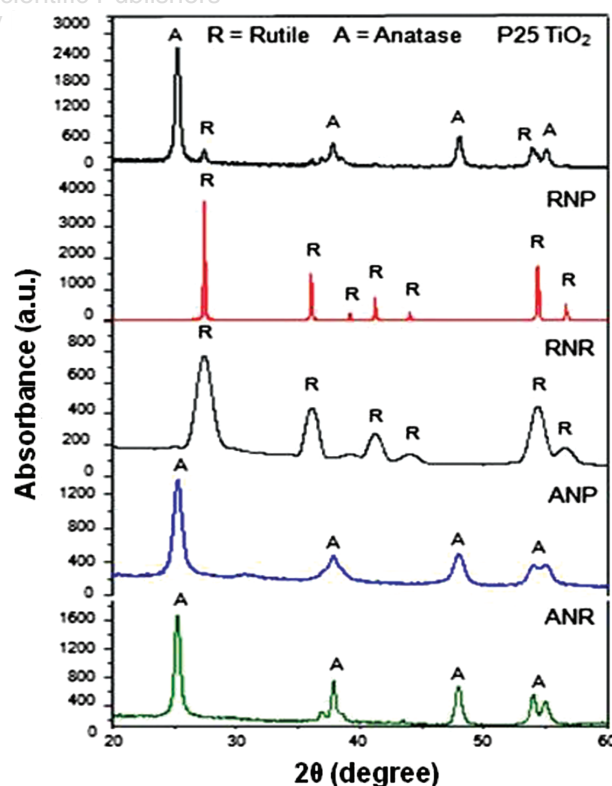


**Figure 1.** XRD patterns of as prepared titania nanoparticles of different morphology.

method using a Smart Sorb 92/93 instrument after pre-heating 100 mg of samples at 150 °C for 1 hour. The time resolve photoluminescence spectra was measured by time-correlated single photon counting (TCSPC) set up by Edinburgh FL920 model at room temperature on excitation with diode lasers at 390 nm in ethanol suspension. The average lifetime ( $\tau_{av}$ ), is related to band edge lifetime  $\tau_1$  and trapping or defect's states given by the following equation

$$\tau_{av} = (a_1\tau_1 + a_2\tau_2)/a_1 + a_2$$

where,  $a_1$  and  $a_2$  denote the amplitude of band edge excitonic and trapping state emission, respectively.

### 2.7. Photocatalytic Activity for Nitroaromatic Reduction

The photoreduction was carried out in a test tube containing 50 mg of TiO<sub>2</sub> powder suspended in 5 ml isopropanol (50 vol%) and 5 mM of nitroaromatic compound (25  $\mu$ mol) in argon atmosphere under continuous magnetic stirring and UV light irradiation. The reaction solution after nitroaromatic photoreduction was centrifuged, filtered through cellulose filter (0.22  $\mu$ m) and product was analysed by HPLC [Agilent 1120 Compact LC equipped with a Qualisil BDS C-18 column

(250 mm  $\times$  4.6 mm, 5  $\mu$ m)] at  $\lambda = 254$  nm with a flow rate of 1 mL/min using MeOH:H<sub>2</sub>O (70:30) as mobile phase and by Gas chromatography-mass spectroscopy (GC-MS-QP 2010 plus) using RTX-5Sil-MS column (15 m  $\times$  0.25 mm  $\times$  0.25  $\mu$ m).

## 3. RESULTS AND DISCUSSION

### 3.1. Structural Analysis

Crystalline phase of P25 TiO<sub>2</sub> and as prepared samples was analyzed by using XRD and are shown in Figure 1. XRD profile of RNP shows highly intense peaks of rutile titania whereas RNR exhibited comparatively less intense peaks of rutile phase at  $2\theta = 27.5^\circ, 36.5^\circ, 41^\circ, 54.1^\circ$  and  $56.5^\circ$  and are assigned to the (110), (101), (200), (111), (210), (211) and (220) planes (JCPDS no. #21-1276). However, ANP and ANR exhibited diffraction peaks at  $2\theta = 25.4^\circ, 37.9^\circ, 47.9^\circ, 53.9^\circ$  and  $54.9^\circ$  are assigned to (101), (004), (200), (105) and (211) planes (JCPDS no. #21-1272) of anatase phase. BET surface area analysis exposed that surface of P25 is  $45 \text{ m}^2\text{g}^{-1}$  while that of ANP and ANR exhibited increased surface area of  $89 \text{ m}^2\text{g}^{-1}$  and  $71 \text{ m}^2\text{g}^{-1}$ , respectively. The surface area of RNP is  $18 \text{ m}^2\text{g}^{-1}$  while it is increases to  $69 \text{ m}^2\text{g}^{-1}$  for RNR.

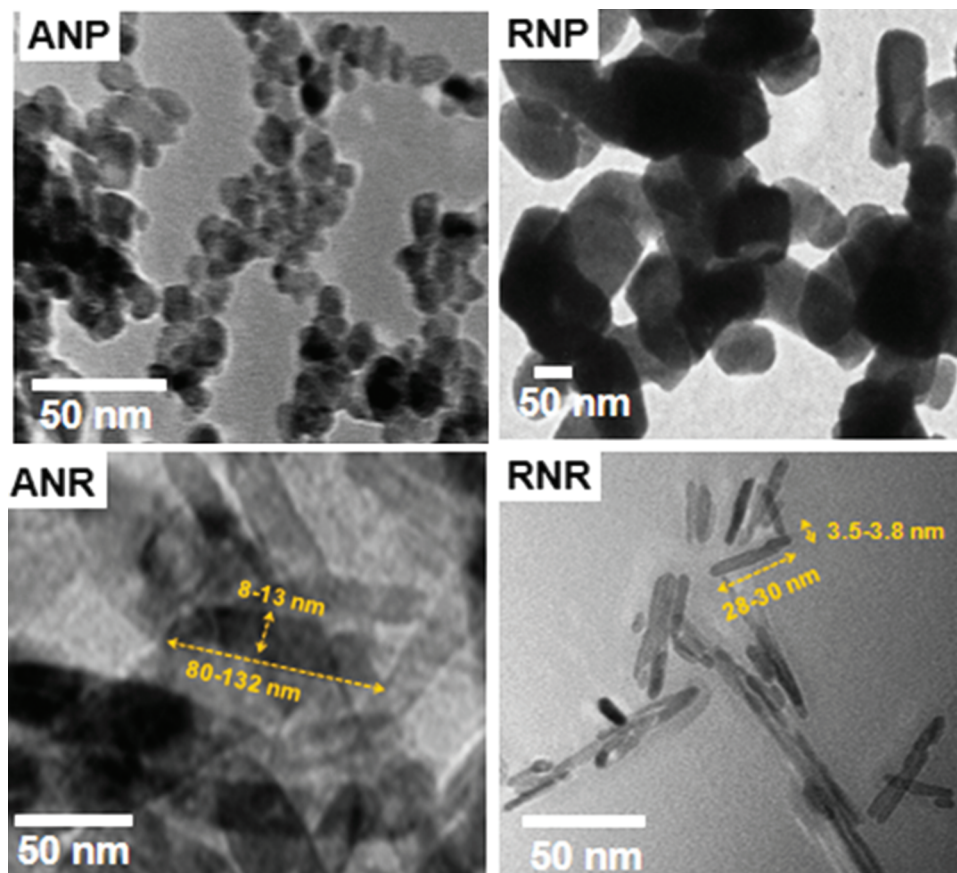


**Figure 2.** TEM images of as prepared titania nanostructures (ANP = anatase nanoparticles, RNP = rutile nanoparticles, ANR = anatase nanorods, RNR = rutile nanorods).

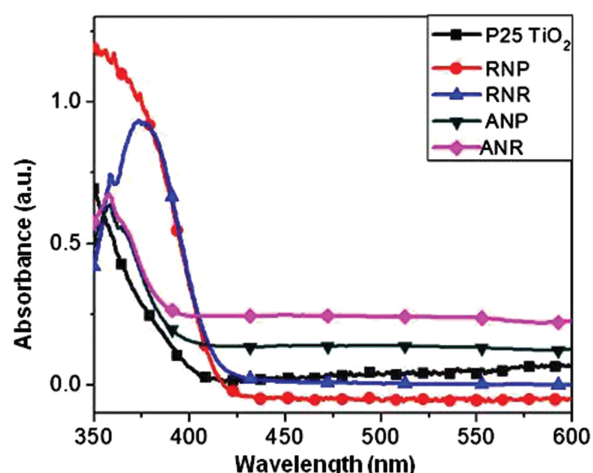


**Figure 3.** Optical absorption spectra of different titania nanostructures.

### 3.2. Morphological Analysis

Morphology of the prepared samples was investigated through TEM analysis. TEM image of P25-TiO<sub>2</sub> exhibited spherical nanoparticles of average size 25–30 nm, RNP also exhibited spherical particles with the size of 120–130 nm while RNR exhibited rod like morphology with the size range ( $L \times W = 28\text{--}30\text{ nm} \times 3.5\text{--}3.8\text{ nm}$ ) as shown in Figure 2. TEM micrographs of ANP shows spherical nanoparticles of average size 8–10 nm and ANR shows the formation of rice like nanorods with size ( $L \times W = 80\text{--}132\text{ nm} \times 8\text{--}13\text{ nm}$ ).

### 3.3. Optical Properties

Optical properties of as prepared TiO<sub>2</sub> samples were studied by recording UV-vis absorption spectra and emission spectra. In Figure 3 absorption onset of P25-TiO<sub>2</sub> appears at 386 nm, whereas the absorption onset for ANP and ANR is blue shifted to 380 and 384 nm respectively. However, the absorption onset of RNP occurs at 413 nm which is further red shifted to 418 nm in RNR. Further, the band gap values of all these samples were calculated from Tauc

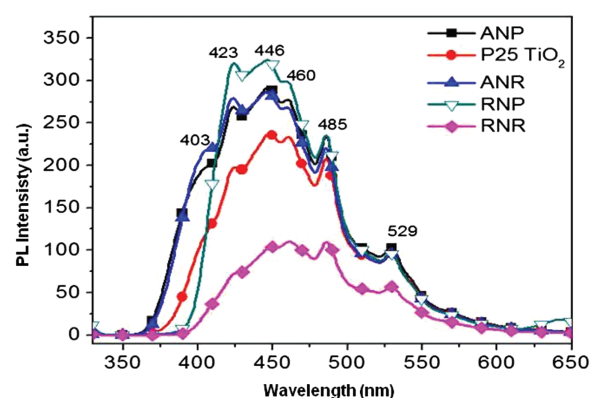


**Figure 5.** Photoluminescence spectra of various titania nanostructures.

plot using the equation

$$\alpha h\nu = A(h\nu - E_g)^n$$

where  $\alpha$  = absorption coefficient,  $h\nu$  = energy of photon,  $A$  = constant,  $E_g$  = band gap of the material and  $n$  = index and its value depends upon on the nature of the electronic transition responsible for the absorption ( $n = 2$  for indirect,  $1/2$  for direct band gap).

The band gap of the samples were calculated by extrapolating the straight-line portion of  $\alpha h\nu$  versus  $E_g$  graph to the  $x$ -axis as shown in Figure 4(a). The band gap values varies from 3.0 eV for RNP to 3.21 eV for ANR (Fig. 4(b)) depending upon the phase and morphology. The low band gap exhibited by RNP and RNR expected to facilitate the efficient electron transfer and may serve as an efficient photocatalyst.

The emission in nanocrystalline TiO<sub>2</sub> is due to the defects resulting from under coordinated Ti<sup>4+</sup> ions, oxygen vacancies, chemisorbed surface species, which result in the localized intra-band gap states that serve as electron traps. The photoluminescence (PL) spectra in Figure 5 showed that TiO<sub>2</sub> nanostructures exhibit the emission bands from 400 to 550 nm range which indicates the occurrence of various surface defect sites. The emission peak, 403 nm,

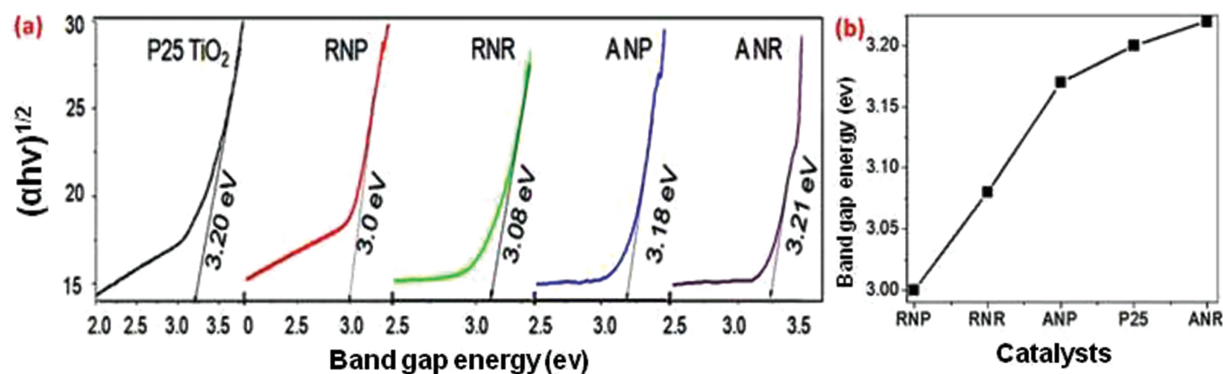


**Figure 4.** (a) The plot of  $(\alpha h\nu)^{1/2}$  function versus the band gap energy of various titania samples (b) variation in the band gap energy of titania samples.

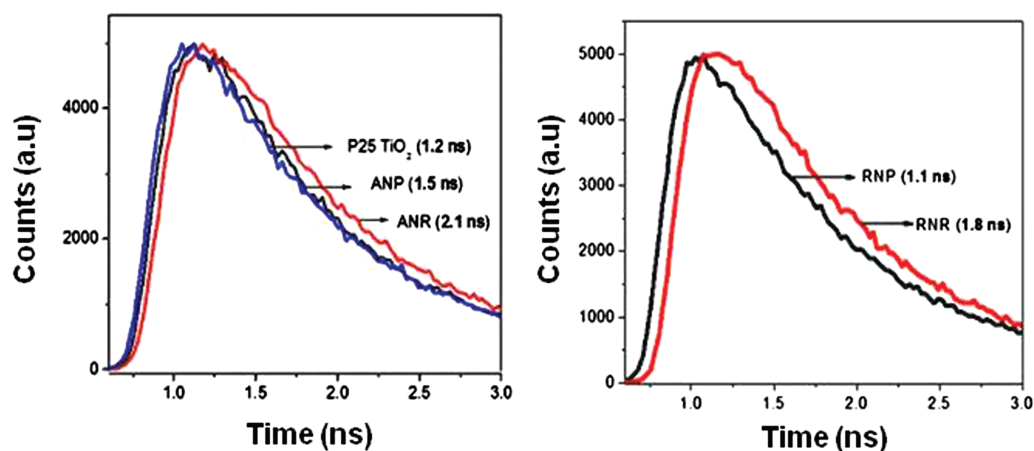


**Figure 6.** Time resolved decay curves of titania nanostructures.

corresponds to a direct band emission of the fundamental band gap (3.2 eV) of anatase  $\text{TiO}_2$ , whereas the emission peak, 423 nm, is attributed to the self trapped excitons. The peak, 446 nm, relates to the emission process of oxygen vacancy defects in  $\text{TiO}_2$  and the emission signal, 485 nm corresponds to the charge-transfer from  $\text{Ti}^{3+}$  to oxygen anion in a  $\text{TiO}_6^{8-}$  complex, related with oxygen vacancies at the  $\text{TiO}_2$  surface.<sup>35–38</sup> The emission, 529 nm, can be related with anion vacancies on the surface of  $\text{TiO}_2$  nanoparticles. The strong quenching in PL emission, in the case of RNR nanoparticles, has been attributed to the decrease in recombination rate of photo-generated electron–hole pairs. The average lifetime<sup>39</sup> of photoexcited  $e^-/h^+$  pairs is calculated by time resolved fluorescence

decays (Fig. 6) has been found to be gradually increased as 1.2, 1.5 and 2.1 ns for P25  $\text{TiO}_2$ , ANP, ANR and respectively, confirming better delocalization of  $e^-h^+$  pairs in the lengthy crystalline NR. Also, average lifetime of RNP and RNR found to be 1.1 and 1.8 ns respectively.

### 3.4. Photocatalytic Study

The photocatalytic activity of as prepared titania catalysts were evaluated by monitoring the photoreduction of *m*-NBA and *m*-NT. Figure 7(a) showed the selective reduction of *m*-NBA to *m*-ABA after 6 h UV irradiation with P25- $\text{TiO}_2$ , ANP and ANR catalysts. It found that smaller ANP (8 nm) catalysts exhibits highest photoactivity for *m*-NBA reduction and produces *m*-ABA with 42% yield

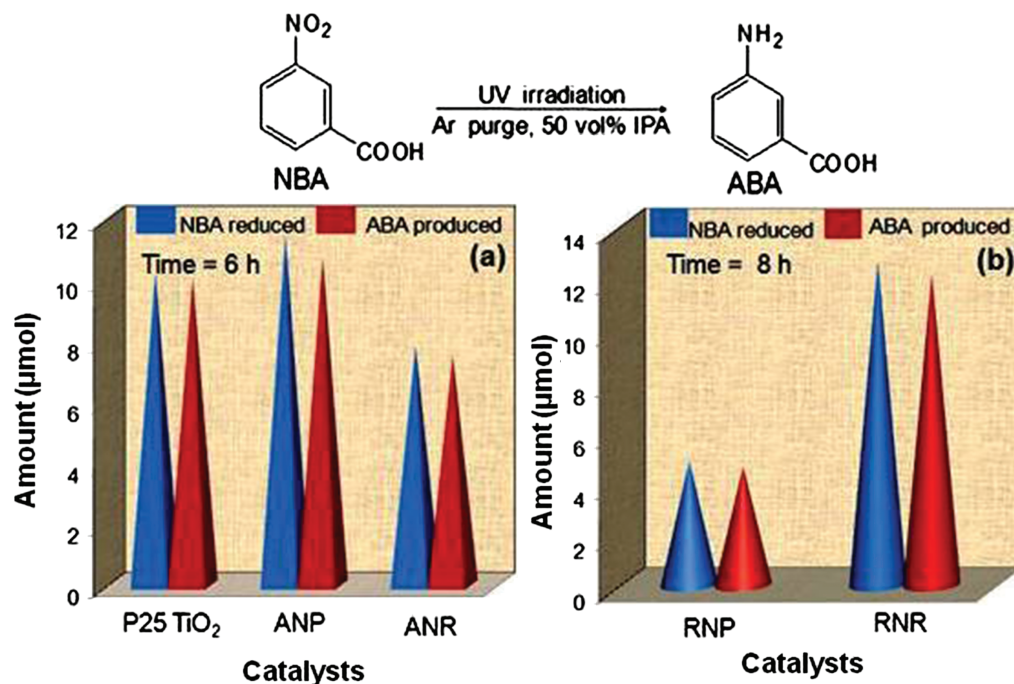


**Figure 7.** *m*-NBA reduction under UV light irradiation by (a) P25- $\text{TiO}_2$ , ANP and ANR for 6 h (b) RNP and RNR for 8 h.

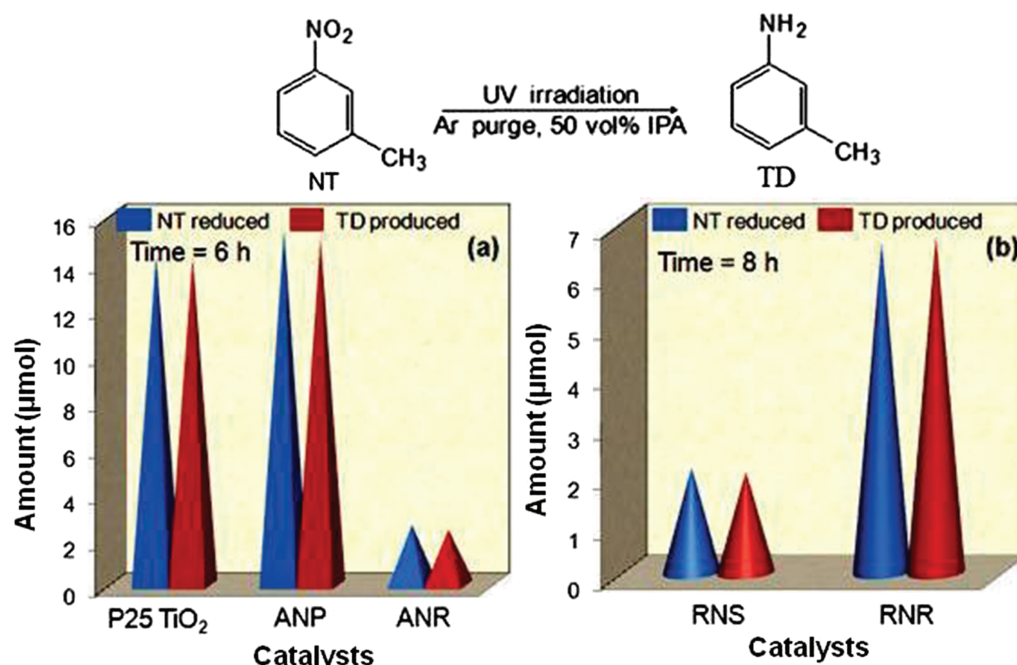


**Figure 8.** *m*-NT reduction under UV light irradiation by (a) P25-TiO<sub>2</sub>, ANP and ANR for 6 h (b) RNP and RNR for 8 h.

as compared to 40% and 30% yield of P25 TiO<sub>2</sub> and ANR respectively. It could be probably due to increased surface area of ANP (89 m<sup>2</sup>g<sup>-1</sup>) owing to its smaller size as compare to 45 m<sup>2</sup>g<sup>-1</sup> and 71 m<sup>2</sup>g<sup>-1</sup> of P25 TiO<sub>2</sub> and ANR respectively. Figure 7(b) showed the significant higher photoactivity for RNR (~3 times) as compared to RNP for *m*-NBA reduction into ABA under 8 h UV irradiation. The yield of *m*-ABA significantly increases upto 48% with RNR as compare to 18% with RNP catalysts. It could be attributed due to long distance electron transport along longitudinal length, higher surface area (69 m<sup>2</sup>g<sup>-1</sup>) of RNR available for adsorption and reduction of *m*-NBA as compare to lesser (18 m<sup>2</sup>g<sup>-1</sup>) surface area of RNP. Also, by changing the morphology from RNP to RNR the charge carrier time also enhances from 1.1 to 1.8 ns which also contributes to its enhanced photoactivity. Also, the obtained results shows that anatase titania nanostructures shows higher photoactivity in lesser irradiation time as compare to rutile nanostructures.

Further Figure 8(a) also shows the same trend for *m*-NT reduction into *m*-toluidene (*m*-TD). It shows that ANP showed highest photoactivity for the reduction of *m*-NT and produces *m*-TD with yield 60% under 6 h of UV irradiation. Also, RNR gives yield 26 % (~3 times) as compare to 8% yield with RNP catalysts (Fig. 8(b)) during 8 h UV irradiation. Figure 8 shows that rate of reduction/hour for *m*-NBA and *m*-NT reduction with various catalysts follows the trend ANP > P25 TiO<sub>2</sub> > RNR > ANR > RNP. This can be attributed to the fact<sup>40-42</sup> that reduction plane {011} related with anatase nanostructures contains a rich array of defects in comparison with reduction plane {110} of R-TiO<sub>2</sub>. The defect sites are identified as Ti<sup>3+</sup> which

behave as an active site on the TiO<sub>2</sub> surface and are necessary for adsorption and the conversion of nitro group to amine.

#### 4. CONCLUSION

It is demonstrated that as prepared RNP, RNR, ANP, ANR could be potentially utilized for nitroaromatics photoreduction. RNR showed superior photoactivity (~3 times) as compared to RNP for the photoreduction of *m*-NT into *m*-toluidine (*m*-TD) and *m*-NBA into *m*-aminobenzoic acid (*m*-ABA) under 8 h UV irradiation. The obtained results show that the long distance electron transport along longitudinal length, larger surface area, quenched PL emission, increased lifetime of charge carriers of RNR as compare to RNP having lower surface area and charge carrier lifetime collectively contribute to its enhanced photocatalytic activity. Furthermore, ANP also shows higher photocatalytic activity than ANR owing to their smaller size and larger surface area as compare to ANR and P25-TiO<sub>2</sub> for *m*-NBA and *m*-NT photoreduction under 6 h UV light irradiation.

**Acknowledgment:** The authors are thankful to Department of Science and Technology, India (SR/NM/NS-40/2008) and council of Scientific and Industrial Research (CSIR), India for providing the financial support.

#### References and Notes

- H. Hirakawa, M. Katayama, Y. Shiraishi, H. Sakamoto, K. Wang, B. Ohtani, S. Ichikawa, S. Tanaka, and T. Hirai, *ACS Appl. Mater. Interfaces* 7, 3797 (2015).

2. M. Boronat, P. Concepcion, A. Corma, S. Gonzalez, F. Illas, and P. Serna, *J. Am. Chem. Soc.* 129, 16230 (2007).
3. O. V. Makarova, T. Rajh, M. C. Thurnauer, A. Martin, P. A. Kemme, and D. Crokek, *Environ. Sci. Technol.* 34, 4797 (2000).
4. X. Pan and Y. J. Xu, *ACS Appl. Mater. Interfaces* 6, 1879 (2014).
5. P. F. Vogt and J. J. Gerulis, *Ullmann's Encyclopedia of Industrial Chemistry, Aromatic Amines*, Wiley-VCH, Verlag GmbH & Co. KGaA, Weinheim (2005), Vol. 2.
6. L. Ying, C. Jixiang, and Z. Jiyan, *Chin. J. Chem. Eng.* 15, 63 (2007).
7. D. He, X. D. Jiao, P. Jiang, J. Wang, and B. Q. Xu, *Green Chem.* 14, 111 (2012).
8. Y. Zheng, K. Ma, H. Wang, X. Sun, J. Jiang, C. Wang, R. Li, J. Ma, *Catal. Lett.* 124, 268 (2008).
9. F. C. Lizana, S. G. Quero, N. Perret, M. A. Keane, *Catal. Lett.* 127, 25 (2009).
10. Y. Chen, J. Qiu, X. Wang, and J. Xiu, *J. Catal.* 242, 227 (2006).
11. H. Rojas, G. Borda, P. Reyes, M. Brijaldo, and J. Valencia, *J. Chil. Chem. Soc.* 56, 793 (2011).
12. D. P. He, H. Shi, Y. Wu, and B. Q. Xu, *Green Chem.* 9, 849 (2007).
13. J. J. Chen, W. K. Wang, W. W. Li, D. N. Pei, and H. Q. Yu, *ACS Appl. Mater. Inter.* 7, 12671 (2015).
14. A. Corma and P. Serna, *Science* 313, 332 (2006).
15. H. Zhu, X. Ke, X. Yang, S. Sarina, and H. Liu, *Angew. Chem.* 122, 9851 (2010).
16. M. S. Wrighton, *Chem. Eng. News* 57, 29 (1979).
17. M. A. Fox, *Nouv. J. Chim.* 11, 129 (1987).
18. T. Kanno, T. Oguchi, H. Sakuragi, and K. Tokumm, *Tetrahedron Lett.* 21, 467 (1980).
19. J. A. Dean, *Handbook of Organic Chemistry*, McGraw Hill, New York (1987), Vol. 8.
20. F. Mahdavi, T. C. Bruton, and Y. Li, *J. Org. Chem.* 58, 744 (1993).
21. C. J. Li, G. R. Xu, B. Zhang, and J. R. Gong, *Appl. Catal. B: Environ.* 115, 201 (2012).
22. A. Hakki, R. Dillert, and D. W. Bahnemann, *Phys. Chem. Chem. Phys.* 15, 2992 (2013).
23. Y. Shiraishi, Y. Togawa, D. Tsukamoto, S. Tanaka, and T. Hirai, *ACS Catal.* 2, 2475 (2012).
24. S. C. Li and U. Diebold, *J. Am. Chem. Soc.* 132, 64 (2010).
25. J. Kaur and B. Pal, *Catal. Comm.* 53, 25 (2014).
26. J. Kaur, R. Singh, and B. Pal, *J. Mol. Catal. A: Chemical* 397, 99 (2015).
27. Q. Zhao, M. Li, J. Chu, T. Jiang, and H. Yin, *Appl. Surf. Sci.* 255, 3773 (2009).
28. J. C. Xu, M. Lu, X. Y. Guo, and H. L. Lia, *J. Mol. Catal. A: Chem.* 226, 123 (2005).
29. J. Yu, H. Yu, B. Cheng, and C. Trapails, *J. Mol. Catal. A: Chem.* 249, 135 (2006).
30. H. J. Yun, H. Lee, N. D. Kim, and J. Yi, *Electrochem. Comm.* 11, 363 (2009).
31. Z. Liu, X. Zhang, S. Nishimoto, M. Jin, D. A. Tryk, T. Murakami, and A. Fujishima, *Langmuir* 23, 10916 (2007).
32. J. N. Nian and H. Teng, *J. Phys. Chem. B* 110, 4193 (2006).
33. K. V. Baiju, S. Shukla, K. S. Sandhya, J. James, and K. G. K. Warriar, *J. Phys. Chem. C* 111, 7612 (2007).
34. A. Dessombz, D. Chiche, P. Davidson, P. Panine, C. Chaneac, and J. P. Jolivet, *J. Am. Chem. Soc.* 129, 5904 (2007).
35. N. D. Abazovic, L. Mirengi, I. A. Jankovic, N. Bibic, D. V. Sojic, B. F. Abramovic, and M. I. Comor, *Nanoscale Res. Lett.* 4, 518 (2009).
36. S. Chaveanghong, S. M. Smith, J. Sudchanham, and T. Amornsakchai, *J. Microsc. Soc. Thail.* 4, 36 (2011).
37. X. Song and L. Gao, *Langmuir* 23, 11850 (2007).
38. J. Liu, J. Li, A. Sedhain, J. Lin, and H. Jiang, *J. Phys. Chem. C* 112, 17127 (2008).
39. S. Khanchandani, S. Kundu, A. Patra, and A. K. Ganguli, *J. Phys. Chem. C* 116, 23653 (2012).
40. U. Aschauer and A. Selloni, *Phys. Chem. Chem. Phys.* 14, 16595 (2012).
41. X. Peng and A. Chen, *Appl. Phys. A* 80, 473 (2005).
42. B. S. Shirke, P. V. Korake, P. P. Hankare, S. R. Bamane, and K. M. Garadkar, *J. Mater. Sci: Mater. Electron* 22, 821 (2011).

Received: 20 March 2017. Accepted: 10 February 2018.